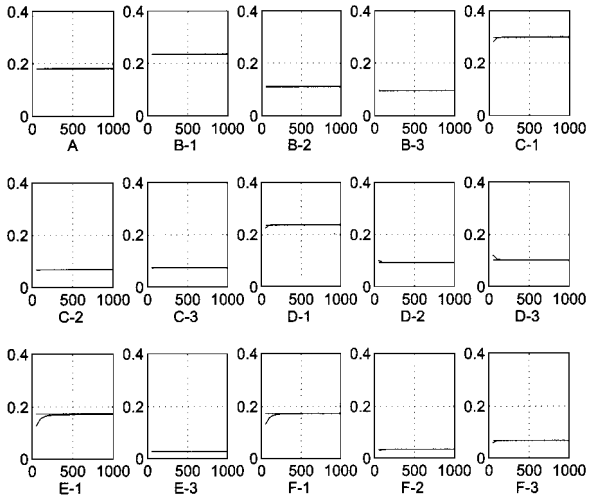

Fig. 1 Phugoid frequency ω_p in rad/s (y axis) vs U_1 in ft/s (x axis).

where

$$A = U_1 - Z_{\dot{\alpha}}$$

$$B = -(U_1 - Z_{\dot{\alpha}})(X_u + M_q) - Z_\alpha - M_{\dot{\alpha}}(U_1 + Z_q)$$

$$C = X_u[M_q(U_1 - Z_{\dot{\alpha}}) + Z_\alpha + M_{\dot{\alpha}}(U_1 + Z_q) + M_q Z_\alpha - Z_u X_\alpha + M_{\dot{\alpha}} g \sin\Theta_1 - M_\alpha(U_1 + Z_q)] \quad (5)$$

$$D = g\sin\Theta_1(M_\alpha - M_{\dot{\alpha}}X_u) + g\cos\Theta_1[Z_u M_{\dot{\alpha}} + M_u(U_1 - Z_{\dot{\alpha}})] - M_u X_\alpha(U_1 + Z_q) + Z_u X_\alpha M_q + X_u[M_\alpha(U_1 + Z_q) - M_q Z_\alpha]$$

$$E = g\cos\Theta_1(M_\alpha Z_u - Z_\alpha M_u) + g\sin\Theta_1(M_u X_\alpha - X_u M_\alpha)$$

The results are plotted in Fig. 1 for the 15 different cases. In each plot, the ordinate shows ω_p and the abscissa shows U_1. Each graph is labeled according to the aircraft and the flight condition it represents. For instance, E-3 denotes aircraft E in flight condition 3. Uniformity is maintained in the graphs by ensuring that all of their ordinates vary from 0 to 0.4. The abscissa of each graph varies from 0 to 1000 ft/s.

It can be seen from the figure that the approximation and the exact value are indistinguishable except at the left extremity. Except for the left extremity, Fig. 1 shows that the phugoid frequency is independent of the forward speed. On close scrutiny, it is seen that the region in which there appears to be a discrepancy between the exact and the approximate values lies below 100 ft/s. Introspection reveals that any speed falling below this limit lies below the stalling speeds of all the aircraft considered in the simulation. Thus, as far as practical flight is concerned, the difference between the exact solution to the phugoid frequency and the approximate solution represented by Eq. (2) is immaterial. This strongly supports Conjecture B.

This suggests that it is not speed, but the change of aerodynamic derivatives with speed, that causes the change in the phugoid frequency. In most cases, the aerodynamic derivatives vary in such a manner as to reduce the phugoid frequency when the speed is increased, leading to widespread belief in Conjecture A.

Conclusion

The notion of yore that the phugoid frequency is inversely proportional to the forward speed is disproved. Counterexamples where the phugoid frequency increases as the forward speed is increased are cited. Using an expression for the phugoid frequency developed by the authors, we have shown that the phugoid frequency is independent of the forward speed, provided the aerodynamic and thrust derivatives are held fixed by some artificial means.

References

[1] Roskam, J., *Airplane Flight Dynamics and Automatic Flight Controls*, 2nd ed., Vol. 1, Roskam Aviation and Engineering Corp., Lawrence, KS, 1979.

[2] Lanchester, F. W., *Aerodonetics*, Constable, London, 1908.

[3] Heffley, R. K., and Jewell, W. F., "Aircraft Handling Qualities Data," NASA CR 2144, 1972, p. 201.

[4] Kamesh, S., and Pradeep, S., "The Phugoid Approximation Revisited," *Journal of Aircraft* (to be published).

Direct Adaptive Control for Gravity-Turn Descent

Colin R. McInnes*
University of Glasgow, Glasgow, Scotland G12 8QQ, United Kingdom

I. Introduction

GRAVITY-TURN descent has been investigated widely[1–4] and used in practice[5,6] for terminal descent to lunar and planetary surfaces. Initial studies of this descent method utilized simple linear feedback control laws to track predefined velocity-range descent profiles. It has been shown that these linear methods can be improved by using nonlinear transformation methods to artificially linearize the system error dynamics.[7] However, all of these control laws require knowledge of key system parameters such as the local gravitational acceleration. In addition, the control laws are not robust to parameter variations or to unmodeled disturbances such as thruster failure. A direct adaptive control law is presented that provides robust tracking of a predefined descent profile. It is shown that the control law is a function only of the lander velocity and altitude and does not require any model-dependent parameters. Because of this inherent robustness, the control law is able to adapt to realistic thruster failure modes such as thruster valves jammed open or closed. Last, because explicit on-line parameter estimation is not required, the control law is computationally efficient, and so it appears attractive for onboard implementation.

II. Gravity-Turn Descent

Gravity turn is a simple descent method whereby the lander thrust vector is aligned opposite to its velocity vector at all points along the descent trajectory. This requirement can be implemented easily onboard by using the attitude control system to null body rates about the lander velocity vector. It can be shown that the method is also near optimal in providing minimum-fuel descents. Although the thrust-vector orientation is fixed, the thrust magnitude can be modulated to track predefined velocity–altitude or velocity–slant range descent profiles. The method also has the useful property that a vertical landing is guaranteed. For terminal descent maneuvers, the planar translational dynamics of the lander may be modeled as a point mass moving over a flat surface with a uniform local gravitational acceleration g, viz.,

$$\dot{v} = ng + g\cos\psi \quad (1a)$$

$$v\dot{\psi} = -g\sin\psi \quad (1b)$$

$$\dot{h} = -v\cos\psi \quad (1c)$$

where the lander state variables are illustrated in Fig. 1. The altitude h can be obtained by a simple radar altimeter and the lander velocity components obtained from a multibeam Doppler radar. These components also provide the lander flight-path angle ψ. The only control

Received June 3, 1998; revision received Aug. 26, 1998; accepted for publication Aug. 30, 1998.

*Reader, Department of Aerospace Engineering. E-mail: colinmc@aero.gla.ac.uk.

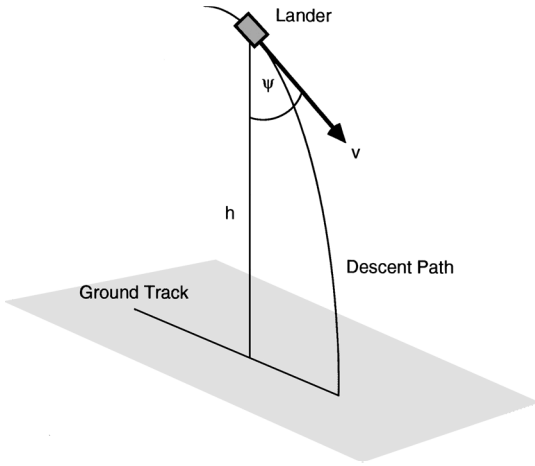

Fig. 1 Schematic geometry of a gravity-turn descent.

variable is the vehicle thrust-to-weight ratio n, which is modulated by throttling the descent thrusters.

III. Direct Adaptive Control

Before the gravity-turn control law is developed, a general direct adaptive control law is presented. This particular adaptive control law[8] is well suited to spacecraft applications because explicit on-line parameter estimation is not required. The control-law gains are adjusted directly in response to the changing behavior of the system dynamics.

Theorem: Consider the following first-order linear system:

$$\dot{x}(t) = ax(t) + bu(t) + d \tag{2}$$

where a, b, and $d \in \Re$ are assumed to be unknown except for the sign of b, which is assumed to be positive. A control law now is required that has the property that $x(t) \to 0$ as $t \to \infty$ without knowledge of a, b, and d. It can be shown that the control law

$$u(t) = -\kappa_1(t)x(t) - \kappa_2(t) \tag{3}$$

possesses these properties, where the control gains are obtained from

$$\dot{\kappa}_1(t) = \tau_1 x^2(t) \tag{4a}$$

$$\dot{\kappa}_2(t) = \tau_2 x(t) \tag{4b}$$

with the parameters $\tau_1, \tau_2 > 0$. A detailed proof of this theorem is presented in Ref. 8, using Lyapunov methods.

IV. Adaptive Gravity-Turn Control Law

Now that the general first-order control law has been presented, an adaptive gravity-turn control law is developed. An adaptive control law is desirable for descent guidance to compensate for unmodeled dynamics and to cope with thruster failures during the descent maneuver. It is assumed that the control law is to track a predefined velocity–altitude profile given by

$$\tilde{v}(h) = \tilde{v}_o[1 - \exp(-\lambda h)] \tag{5}$$

This function provides a constant descent speed $\tilde{v}_o$ with exponential braking prior to soft landing. The braking is defined by the shaping parameter λ, which then is related to the maximum thrust/weight ratio required during the nominal descent.[9] A velocity error ε now is defined as

$$\varepsilon = v(t) - \tilde{v} \tag{6}$$

Then, using this definition with Eq. (1a), the error dynamics of the system can be written as

$$\dot{\varepsilon} = (\tilde{v}' \cos\psi)\varepsilon + ng + (g\cos\psi + \tilde{v}'\tilde{v}\cos\psi) \tag{7}$$

where $\tilde{v}'$ is the derivative of $\tilde{v}$ with respect to h. It can be seen that Eq. (7) is now in the form of Eq. (2), with the nonlinear terms grouped as an unknown disturbance. The lander control law then can be written as

$$\tilde{n}(v, h) = -(1/g)\{\kappa_1(t)[v(t) - \tilde{v}(h)] + \kappa_2(t)\} \tag{8}$$

where the gains again are obtained from

$$\dot{\kappa}_1(t) = \tau_1[v(t) - \tilde{v}]^2 \tag{9a}$$

$$\dot{\kappa}_2(t) = \tau_2[v(t) - \tilde{v}(t)] \tag{9b}$$

with the constants $\tau_1, \tau_2 > 0$. It can be seen that the control law is a function only of the lander velocity and altitude. Previous nonlinear control laws[7] also required knowledge of the lander flight-path angle ψ and the local gravitational acceleration g. This adaptive control law is applied now to a typical lander descent control problem with unmodeled dynamics and thruster failure.

V. Results and Discussion

The velocity–altitude profile defined in Eq. (5) is used with a required descent rate $\tilde{v}_o$ of 4 m/s, starting from an altitude of 100 m

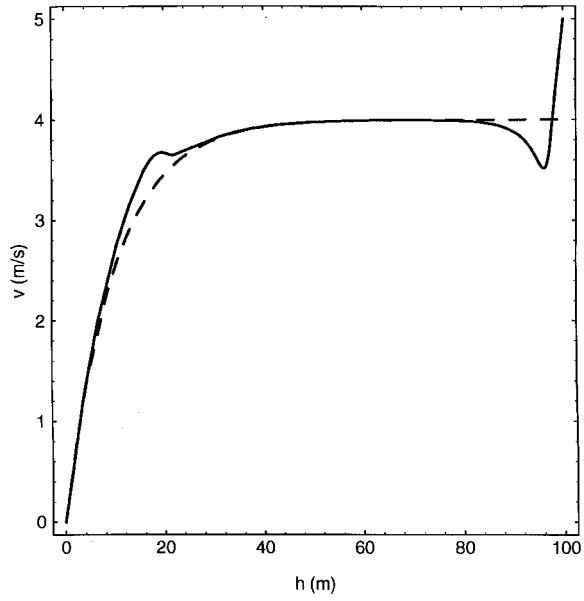

Fig. 2a Velocity–altitude profile tracking (– – –, required profile, and ——, actual profile).

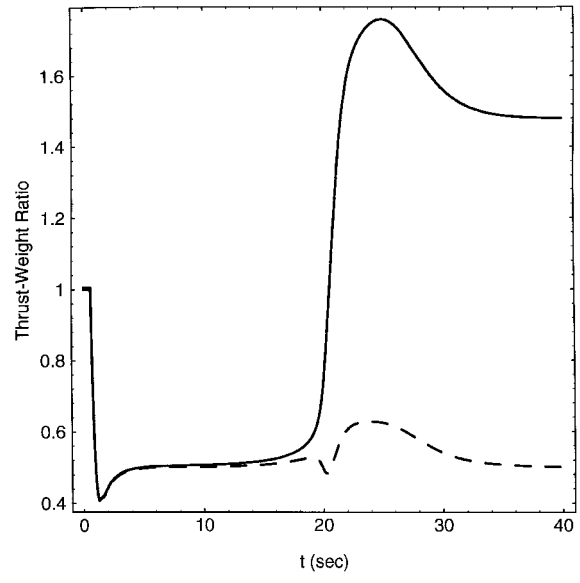

Fig. 2b Thrust-to-weight ratio (– – –, actuated, and ——, commanded).

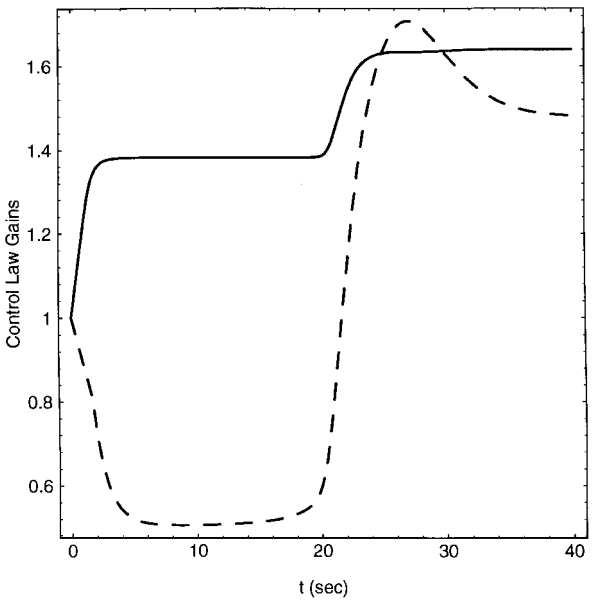

Fig. 3 Adaptive-control-law gains, $\kappa_1(0) = \kappa_2(0) = 1$, $\tau_1 = \tau_2 = 1$ (——, κ_1, and - - -, κ_2).

and flight-path angle ψ of 10 deg. The initial lander velocity is set at 5 m/s to represent residual errors from the previous descent phase. It is assumed that the lander uses clustered descent thrusters and that a set of these thrusters fails with the throttle open, inducing a constant-bias acceleration of $0.5g$. In addition, at the midpoint of the descent maneuver, the remaining thrusters are degraded with the available thrust reduced to one-third of the initial available thrust. This failure mode is modeled by multiplying the commanded thrust by

$$f(t) = \tfrac{2}{3}\left[1 - (1/\pi)\tan^{-1}(2t - t_f)\right] \tag{10}$$

so that the actuated thrust weight ratio becomes $\tilde{n}(v, h) f(t)$.

The descent profile of the lander is shown in Figs. 2a and 2b along with the commanded and actuated thrust weight ratio. It can be seen that the initial velocity error is removed by throttling down the descent thrusters to allow the lander to accelerate and, finally, to track the required descent profile, even in the presence of the 0.5-g bias acceleration. Then, at the midpoint of the maneuver, the available thrust is reduced, as described above. It can be seen from Fig. 3 that the control-law gains adapt to this failure and that after a short transient the lander continues to accurately track the required descent profile. This failure is compensated for by increased demands on the remaining descent thrusters, as seen in Fig. 2b. On landing, the actuated thrust weight ratio is only 0.5 because of the jammed thrusters providing a constant $0.5g$ bias acceleration. Therefore, the lander has a total thrust/weight ratio of unity, as required for a soft landing. It is also found that $\psi \to 0$, so that a vertical landing is ensured.

VI. Conclusions

A direct adaptive control law for gravity-turn descent is presented that is robust and able to compensate for multiple thruster failures. The control-law gains adapt to these failures in direct response to the changing behavior of the system dynamics. Because on-line parameter estimation is not required, the control law is computationally efficient for onboard implementation. Such robust and efficient control laws appear attractive for low-cost planetary or lunar landers, where high controller performance is required, but without significant computational effort.

References

[1]Cheng, R. K., "Lunar Terminal Guidance," *Lunar Missions and Exploration*, edited by C. T. Leondes and R. W. Vance, Wiley, New York, 1964, pp. 308–355.

[2]Citron, S. J., Dunn, S. E., and Meissinger, H. F., "A Terminal Guidance Technique for Lunar Landing," *AIAA Journal*, Vol. 2, No. 3, 1964, pp. 503–509.

[3]Cheng, R. K., "Terminal Guidance for a Mars Softlander," 8th International Symposium on Space Technology and Science, Tokyo, Japan, 1969, pp. 855–865.

[4]McInnes, C. R., "Gravity Turn Descent with Quadratic Air Drag," *Journal of Guidance, Control, and Dynamics*, Vol. 20, No. 2, 1997, pp. 393, 394.

[5]Cheng, R. K., "Design Consideration for Surveyor Guidance," *Journal of Spacecraft and Rockets*, Vol. 3, No. 11, 1966, pp. 1569–1576.

[6]Ingoldby, R. N., "Guidance and Control System Design of the Viking Planetary Lander," *Journal of Guidance and Control*, Vol. 1, No. 3, 1978, pp. 189–196.

[7]McInnes, C. R., "Non-Linear Transformation Methods for Gravity-Turn Descent," *Journal of Guidance, Control, and Dynamics*, Vol. 19, No. 1, 1996, pp. 247, 248.

[8]Hong, J., Bhat, S. P., and Bernstein, D. S., "Adaptive Nonlinear Motion Control," Aerospace Engineering Dept. Internal Rept., Univ. of Michigan, Ann Arbor, MI, March 1998.

[9]McInnes, C. R., "Terminal Descent to the Lunar Surface with Terrain Constraints," *Acta Astronautica*, Vol. 36, No. 7, 1995, pp. 367–377.

Propulsion System Sizing for Orbital Inspection Vehicles

Trevor Williams*
University of Cincinnati, Cincinnati, Ohio 45221
and
Sergei Tanygin†
Analytical Graphics, Inc., Malvern, Pennsylvania 19355

Introduction

THERE is currently growing interest in the development of remotely piloted inspection vehicles capable of performing fly-arounds of the Space Shuttle or of a space station on-orbit. For example, NASA flight tested the AERcam, the autonomous extravehicular activity robotic camera Sprint vehicle[1,2] that is the prototype of a family of spacecraft for Shuttle and International Space Station inspection tasks, during the recent STS-87 mission. This Note describes methods for selecting the two main parameters that describe the propulsion system of such vehicles: the total Δv capacity of the tankage and the thrust level of the jets. Δv requirements are clearly related to the desired mission range and flight duration, as well as attitude control requirements. Choice of thrust level must be made on the basis of a tradeoff between safety and performance, bearing in mind the types of missions to be performed by such a vehicle. As regards safety, too high a thrust may pose unacceptable risks of a high-speed collision in the event that a malfunction on the inspection vehicle causes it to fire toward the mother spacecraft. For instance, if a thruster becomes stuck on, the resulting long-term net linear acceleration may, in some cases,[3] approach the one-jet thrust/mass ratio of the vehicle. On the other hand, too low a thrust level will not permit the vehicle to overcome orbital effects and hover at an appreciable distance above, below, or to the side of the larger spacecraft; such positioning is likely to prove very desirable in future inspection missions.

The safety issues given in the preceding points dictate that inspection vehicles will necessarily be low-thrust spacecraft: accelerations as low 50 μg have been considered.[4] Consequently, extended burns will be required to accelerate up to even moderate relative speeds. The usual assumption of an impulsive Δv is, thus, not valid for this class of spacecraft. Furthermore, these vehicles are initially to be flown by a human operator, essentially by means of visual cues alone. Therefore, low-thrust optimal control techniques that require

Received Jan. 15, 1997; revision received Aug. 17, 1998; accepted for publication Sept. 24, 1998.

*Associate Professor, Department of Aerospace Engineering. Associate Fellow AIAA.

†Senior Astro-Development Engineer, 325 Technology Drive.